Materials Today Chemistry 26 (2022) 101112

Contents lists available at ScienceDirect

Materials Today Chemistry

journal homepage: www.journals.elsevier.com/materials-today-chemistry/

Mechanochemically driven formation of protective carbon films from ethanol environment

A. Shirani [a], Y. Li [a], J. Smith [a], J.F. Curry [b], P. Lu [b], M. Wilson [b], M. Chandross [b], N. Argibay [b], D. Berman [a, *]

[a] Department of Materials Science & Engineering, University of North Texas, Denton, TX 76203, USA
[b] Material, Physical, and Chemical Sciences Center, Sandia National Laboratories, Albuquerque, NM 87123, USA

ARTICLE INFO

Article history:
Received 7 June 2022
Received in revised form
20 July 2022
Accepted 25 July 2022
Available online 28 August 2022

Keywords:
Tribochemistry
Zero wear
Platinum
Catalysis
Graphene

ABSTRACT

Wear and degradation of interfaces remain a significant roadblock in commonly used mechanical assemblies across various industries, resulting in loss of their efficiency and ultimately functionality. To advance the state-of-the-art in tribological applications, new materials must be developed not only to resist degradation, wear, and higher frictional losses in extreme environments (i.e. high temperatures, contact/shear forces, etc.), but also to benefit from them. By adopting hard, catalytic interfaces, a wide range of contact conditions can emerge where mechanochemical interactions lead to the formation of protective or self-healing lubricious films. Here, we demonstrate the mechanochemically driven formation of protective carbon films on Pt-Au alloys during sliding in an ethanol environment. We demonstrate the effect of temperature and contact pressure on film formation. The films formed on Pt-Au alloys exhibit a highly graphitic structure as indicated by Raman and Transmission Electron Microscopy (TEM) analyses. The observed results are further supported by molecular dynamics simulations that show the changes in the dissociation and transformation of ethanol molecules with applied pressure and temperature. The results create a new understanding of transformations in the contact and suggest a solution for addressing tribological challenges in the mechanical systems operated in low viscosity fuels.

1. Introduction

Surface degradation accounts for more than 70% of the loss of functionality in mechanical systems [1,2]. Out of this, 50% is attributed to mechanically induced wear and deformation of materials [3,4]. To address this issue, surfaces are often covered with protective coatings to mitigate wear and frictional losses during sliding [5–7]. Those films, however, eventually wear or experience adhesion and delamination issues without any potential for replacement or repair in the field. This is especially true for films created through more demanding deposition processes requiring high temperature/high vacuum. Consequently, oil-based lubrication has been a traditional approach used by industry to protect the sliding surfaces by delivering the viscous lubricant directly into the sliding contact. However, the new initiatives aiming to operate low carbon emission mechanical systems using low-viscosity fuels made the use of traditional oil lubricants not viable.

Our prior studies demonstrated excellent tribological properties of ordered carbon layers, two-dimensional (2D) graphene [8–11]. Easy shear of 2D layers provides a unique set of characteristics needed for suppressing damage in mechanical contacts [12–16]. Specifically, in the case of graphene platelets lubricating sliding steel counterparts, we observed a 4–5x times reduction in friction and 4 orders of magnitude reduction in wear [10,11]. This improved performance persisted when transitioning between humid and dry environments [9]. However, the replenishment of such coatings also poses certain challenges.

The same contact conditions that lead to the wear and deformation of interfaces (i.e. high contact/shear forces and temperatures) can also provide substantial amounts of mechanical energy to chemical species that appear at the interfaces [17,18]. Subsequently, for substrates that exhibit a high degree of wear resistance and catalytic potential, aggressive contact conditions that otherwise wear or damage substrate surfaces can instead lead to mechanochemical interactions that promote the formation of

* Corresponding author.
E-mail address: diana.berman@unt.edu (D. Berman).

https://doi.org/10.1016/j.mtchem.2022.101112
2468-5194/

protective tribofilms [18–20]. Dynamic processes at the sliding interfaces create favorable temperature and pressure conditions [17,21] that can facilitate a chemical activity on the surface of sliding material, thus significantly reducing the required external energy. These reactions are capable of forming durable, self-generating tribofilms directly at the contact [22–25].

Organic compounds in particular (i.e. ambient or liquid hydrocarbons) have been shown to readily decompose on hard, catalytically active substrates and produce tribofilms with a wide range of intriguing tribological characteristics [26]. For example, the formation of graphitic layers from internal body fluids has been detected in metal-on-metal hip replacements [27]. Additionally, the formation of diamond-like carbon (DLC) films on Pt-Au alloys was observed in a dry sliding environment with trace organics [28]. These films can have a tremendous impact on the performance of mechanical systems, though their formation has

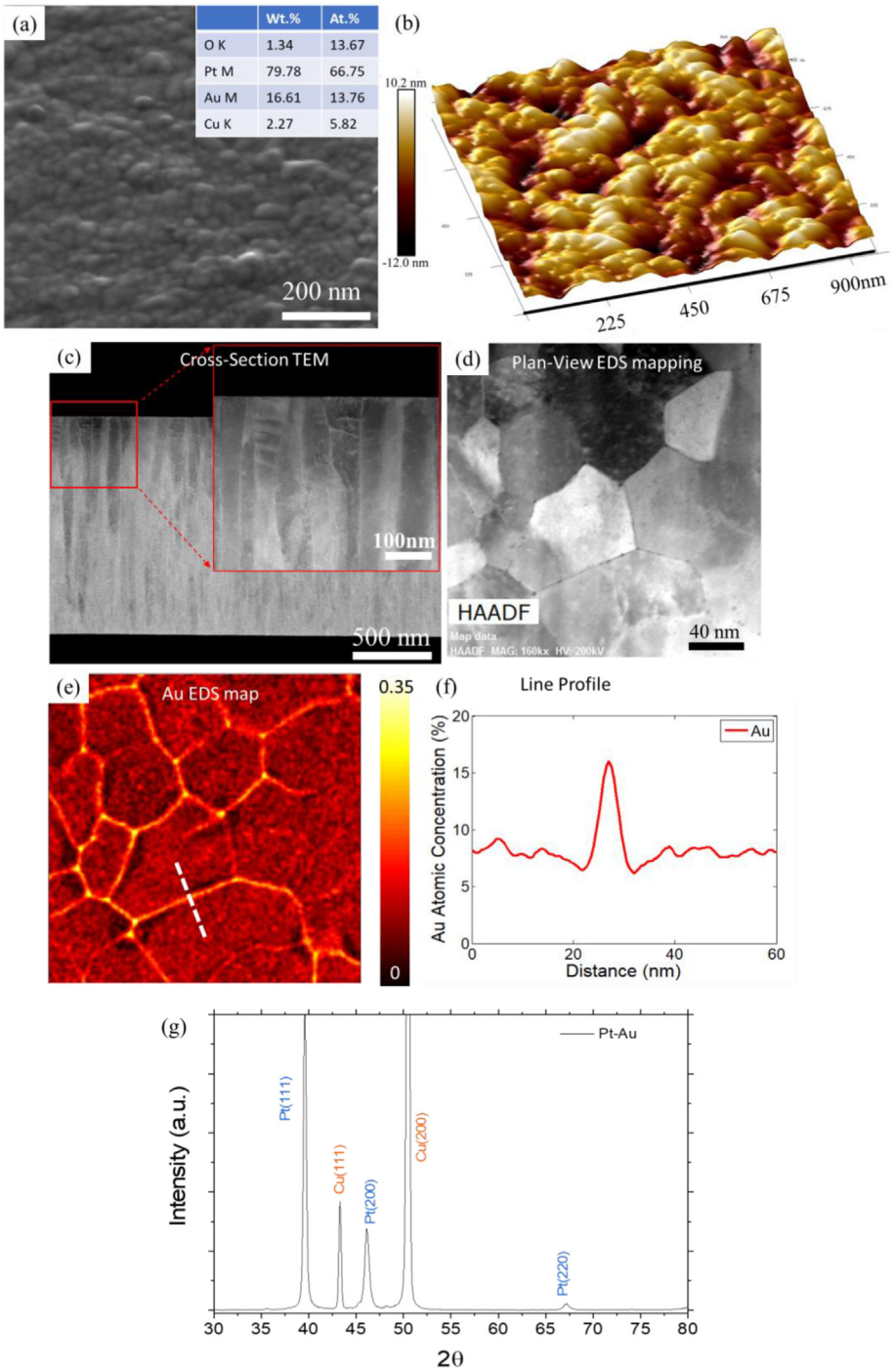

Fig. 1. (a) Deposited Pt-Au films and composition EDS analysis of the coating. (b) 3D height profile AFM image of the coating surface. (c) Cross-sectional TEM and (d) plan-view EDS mapping showing the top view of the grains. (e) EDS mapping and (f) line scan of Au atomic concentration, respectively. (g) XRD pattern of the Pt-Au coating.

only been explored in a limited number of studies to date. Specifically, it has been shown that the presence of catalytically active substrates subjected to sliding in organic species such as vapor phase hydrocarbons or oils initiates the growth of DLC-like films in the wear track that significantly reduced friction and wear of the sliding interfaces [28,29]. Tribologically-induced transformation has been also observed in a dry environment for the carbon-iron system [30]. Tribocatalytically-active iron nanoparticles dispersed on a silicon substrate surface sliding against a DLC counterface facilitated the reconstruction of DLC or amorphous carbon into onion-like carbon (OLC) structures [30].

Here, we demonstrate the mechanochemical formation of lubricious carbon films can be used as a viable approach to addressing the tribological issues of the surfaces operated in low viscosity fuel environments, such as ethanol. For this, we implement Pt-Au coating that upon rubbing facilitates disintegration and reconstruction of hydrocarbon molecules into graphitic carbon film. We show that both temperature and pressure have a critical effect on the rate of tribofilm formation.

2. Experimental procedure

2.1. Deposition of Pt-Au coatings

The samples were deposited on copper substrates by direct current magnetron sputtering in a cryo-pumped high vacuum system (base pressure of ~10^{-7} Torr). Sputtering was performed using high purity Au-Pt deposition targets pre-sputtered for several minutes prior to deposition to prevent the incorporation of adventitious carbon. The coatings, even without further annealing, as analyzed in prior work [28,31], demonstrated a very high hardness of 7.1 ± 0.4 GPa.

2.2. Tribological tests

The tribological assessment of the samples was performed using a macroscale pin-on-disk tribometer (Anton Paar, TRB^3) equipped with a liquid cell of up to 100 ml capacity and a heating stage. Alumina balls of 6.35 mm diameter and initial roughness of ~20 nm Ra were used as the counterpart material. The tests were performed at 25 °C, and 50 °C under ethanol submersion, in a reciprocating mode at 2 Hz over a 2 mm sliding distance. The maximum linear speed was 0.44 cm/s, and the applied load ranged from 0.25 N to 1 N, corresponding to 0.4–0.7 GPa maximum Hertzian contact pressure. Each test was repeated at least 3 times to confirm the reproducibility of the results.

2.3. Characterization

Chemical analysis, elemental mapping, and cross-sectional microscopy were conducted using FEI Quanta 200 SEM equipped with energy-dispersive X-ray spectroscopy (EDS) at 5 kV beam voltage. A focused ion beam (FIB) attachment to the FEI Quanta SEM was used for cross-sectional imaging and TEM sample preparation. High-magnification micrographs were captured with TEM (FEI Tecnai G2 F20). Optical analysis of the wear tracks was performed using a Zeiss optical microscope. Raman spectroscopy analysis was performed using the Renishaw Raman system with a green laser (532 nm). The composition of the coatings and corresponding phases were tested using the Rigaku Ultima III X-ray diffractometer (XRD) with Cu Kα X-ray source operated in θ-2θ scanning mode with 1°/min scanning rate and 0.02° step increments. Additionally, chemical analysis of the wear tracks was performed using X-ray photoelectron spectroscopy (XPS) with a high flux X-ray source with an Aluminum anode for X-ray generation and a quartz crystal

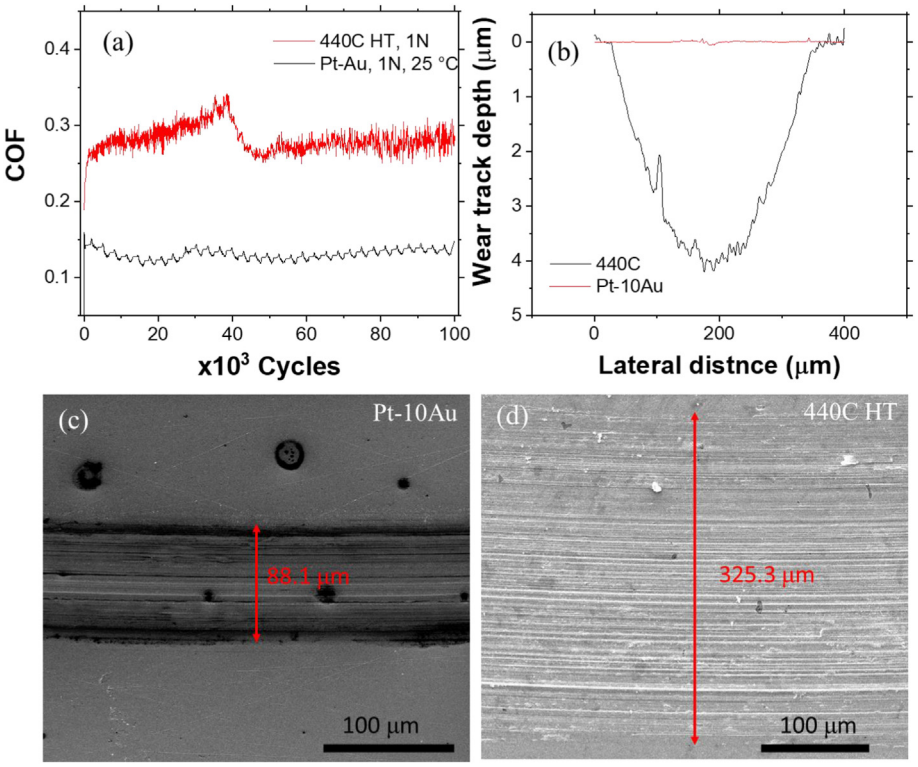

Fig. 2. (a) Coefficient of friction of Pt-Au coating and heat-treated AISI 440 C (with 58–60 HRC hardness) tested against an alumina ball at 1 N load at room temperature. (b) Stylus profilometry results for the wear track depth. Micrographs of the wear track of (c) Pt-Au, (d) AISI 440C HT.

monochromator to focus and scan the beam on the sample with the PHI Versaprobe apparatus. Coating roughness and thickness analysis were performed using Veeco Dektak 150 stylus profilometer with a 2.5 μm tip radius. AFM height profile measurements were performed using Bruker MultiMode 8 microscope in tapping mode with the scan area of 1×1 μm^2 and the scan rate of 0.5 Hz.

2.4. Simulations

Simulations were performed using the LAMMPS simulation code [32] with a reactive force field (ReaxFF) developed for Pt catalysts [33]. One hundred ethanol molecules were placed between pair of 1.6 nm thick single-crystal Pt layers with (001) surface orientation. The Pt layers were sheared at a velocity of 1 m/s with applied loads of 0.5, 1.25, and 2 GPa at temperatures of 300, 500, and 700 K. Temperatures were maintained with a Langevin thermostat. A Langevin thermostat was applied to all mobile atoms (i.e. except those involved in applying forces), but only in the y-direction, perpendicular to the normal (z) and shear (x) directions. In-house post-processing codes were used to identify molecules by searching for user-defined fragments as small subgraphs contained in the global bond information determined by ReaxFF.

3. Results and discussion

The surface morphology of the Pt-Au coating is illustrated in Fig. 1a and b. SEM micrograph and AFM 3D images of the Pt-Au film surface indicate uniform structures. The cross-sectional analysis of the films was performed using TEM. Results indicate that the film of ~1725 ± 10 nm thickness has a columnar structure (Fig. 1c) with grain sizes in the 10–40 nm range, in agreement with the AFM and SEM results (Fig. 1d). TEM EDS map and line scan analysis show Au was deposited preferentially across the grain boundaries (Fig. 1e and f) with Au twice as likely to accumulate at the grain boundaries as within the grains. At grain-boundaries, Au concentration reached up to 15 at%, while the average concentration among the grains was about 7–8 at% (Fig. 1f). According to the high-resolution plan-view TEM, and Au EDS map, Au clusters were formed at the grain boundaries with an average size of less than 5 nm. XRD analysis of the film indicates the formation of (111) and (200) Pt planes

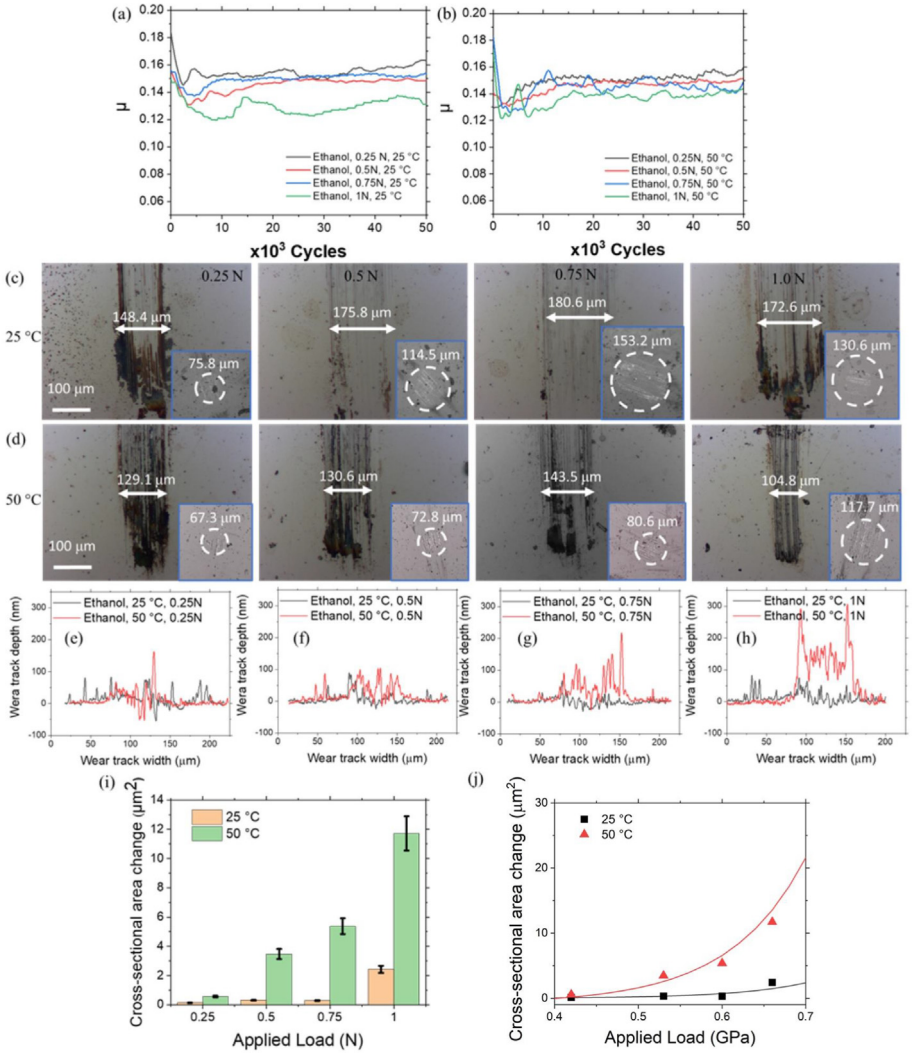

Fig. 3. Tribological analysis of the Pt-Au coating in an ethanol environment at (a) 25 °C and (b) 50 °C. Micrographs of the wear track and inserted counter body for tests performed at (c) 25 °C and (d) 50 °C. Profile of the wear track as a function of testing temperature at 0.25 N (e), 0.5 N (f), 0.75 N (g), and 1 N (h). Calculated film growth on the wear track (i). Experimental and modeled values for the tribofilm growth rate as a function of applied pressure (j) fitted by the Arrhenius model.

(Fig. 1g) and the absence of Au peaks in the XRD spectra further confirms the amorphous structure of the Au segregated at the grain boundaries. This solute segregation approach was deliberate to stabilize the grain boundaries and provide beneficial mechanical properties [28,31].

The tribological characteristics of the Pt-Au film under ethanol lubrication were compared to those of heat-treated (HT) AISI 440C steel with 58–60 HRC hardness (referred to as 440C HT), one of the standard materials used in a wide range of mechanical assemblies such as fuel delivery system components (Fig. 2). A summary of the frictional behavior of the Pt-Au film and uncoated steel sliding against Al_2O_3 in the ethanol environment at 25 °C and 0.64 GPa Hertzian maximum contact pressure is provided in Fig. 2a. The tribology tests were conducted over 100k sliding cycles. The 440C HT shows the average coefficient of friction (COF) of 0.3 with uneven behavior and abrupt spikes around the 30k cycle that indicates plastic deformation, micro-cutting, and formation of debris during the test. Meanwhile, the Pt-Au provides very uniform and steady frictional behavior with the COF ~0.16.

A comparison of the wear tracks reveals the improved wear resistance of the Pt-Au sample over the uncoated steel surface (Fig. 2b). 440C HT, shows deep grooves with 241.8 μm wear track width. However, Pt-Au just has 88.1 μm wear track width without evidence of in-depth wear (Fig. 2c and d). Stylus profilometry results indicate that Pt-Au film experienced almost near zero depth of the wear track, while 440C HT shows 4 μm depth resulting in the wear rate of 3.7 × 10^{-6} mm^3/N m (Fig. 2b).

The Pt-Au metal alloy system has been reported to show highly thermally stable nanocrystallinity [34] that is potentially responsible for the excellent wear resistance of the material [31]. To understand the origin of the superior tribological properties we focus on a detailed analysis of the Pt-Au film. To assess how the Pt-Au film behaves at different contact pressure and temperature conditions, a series of tribology experiments, within the range of the maximum applied Hertzian contact pressure 0.4–0.7 GPa, (0.25–1 N), and at temperatures of 25 °C and 50 °C, were conducted (Fig. 3). The coefficient of friction values are summarized in Fig. 3a and b and show that the Pt-Au film has lower COFs at higher loads. The minimum COF values are roughly 0.13 at 25 °C and 0.16 at 50 °C.

Optical micrographs of the wear track and the counter-body indicate that a higher applied load does not have a considerable effect on the size of the wear track. As the load increased within the 0.25–1 N range, at 25 °C, the wear track width increased by ~16%, from 148.4 μm to 172.6 μm. Surprisingly, at 50 °C, not only did the size of the wear tracks not increase, they rather showed a reduction from 129.1 μm to 104.8 μm as the load was changed from 0.25 N to 1 N, respectively (Fig. 3c and d).

A comparison of the representative wear tracks' profiles from stylus profilometry is shown in Fig. 3e–h. The wear tracks show the accrual of material within the contact, leaving no discernible wear. This suggests the tribocatalytically-activated formation of solid films at the sliding interfaces during shear. Increased temperature and load clearly show a positive effect on the tribofilm formation, with the maximum tribo-film formation at 50 °C and 1 N (Fig. 3h).

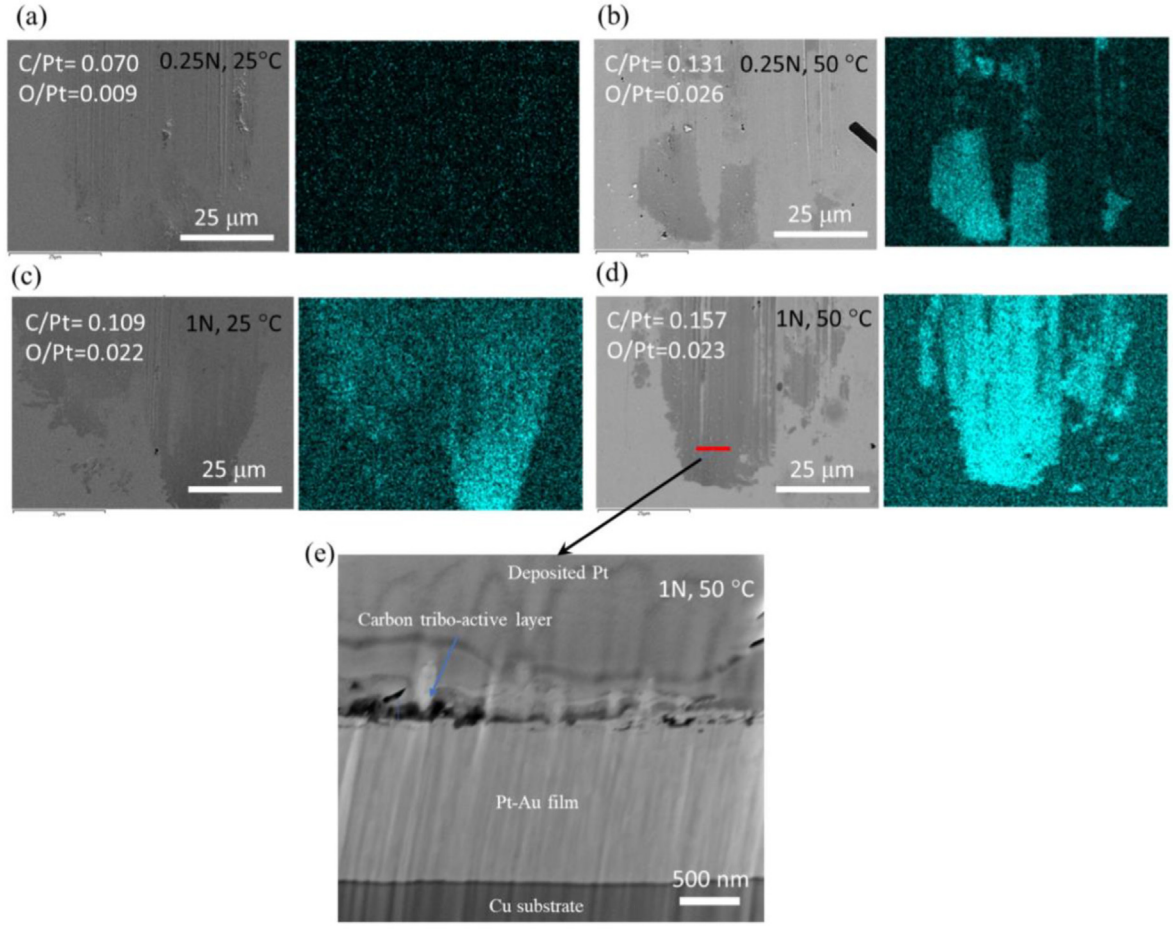

Fig. 4. EDS map analysis of the wear track (SEM image and the corresponding EDS map of carbon intensity) at (a) 0.25 N, 25 °C, (b) 0.25 N, 50 °C, (c) 1 N, 25 °C, and (d) 1 N, 50 °C. (e) FIB-cross sectional view of the tribo-film at the wear track.

To have a better quantitative understanding of the temperature and applied load effects on the formation of protective tribofilms, the cross-sectional area changes are summarized in Fig. 3i. As the profile of the wear track varies depending on the location of the measurements, five profilometry scans were performed away from the edges and the resulting material accumulation has been averaged to estimate the material gain as a function of the load and temperature. These results further confirm that higher temperature and applied load provide more favorable conditions for tribofilm formation. It should be noted that because the films are not uniform the cross-sectional measurements shown are averaged over at least 3 scans performed at the center of the wear tracks.

The observed tribocatalytically-driven formation of the films is fitted by an Arrhenius model (Fig. 3j), suggesting that the growth rate should depend on the temperature and stress as [35,36]:

$$\Gamma = \Gamma_0 \exp(-(\Delta U_{act} - \sigma \Delta V_{act})/k_B T) \quad (1)$$

where the constant Γ_0 depends on the nature of the carbon species, ΔU_{act} is the internal activation energy for the tribofilm formation, σ is the mean value of the stress (here the contact pressure in GPa), ΔV_{act} is the activation volume, k_B is Boltzmann's constant, and T is the absolute temperature. The parameter $\Gamma_0 = V_m \upsilon$ depends on the effective attempt frequency, υ, and the molar volume V_m of the

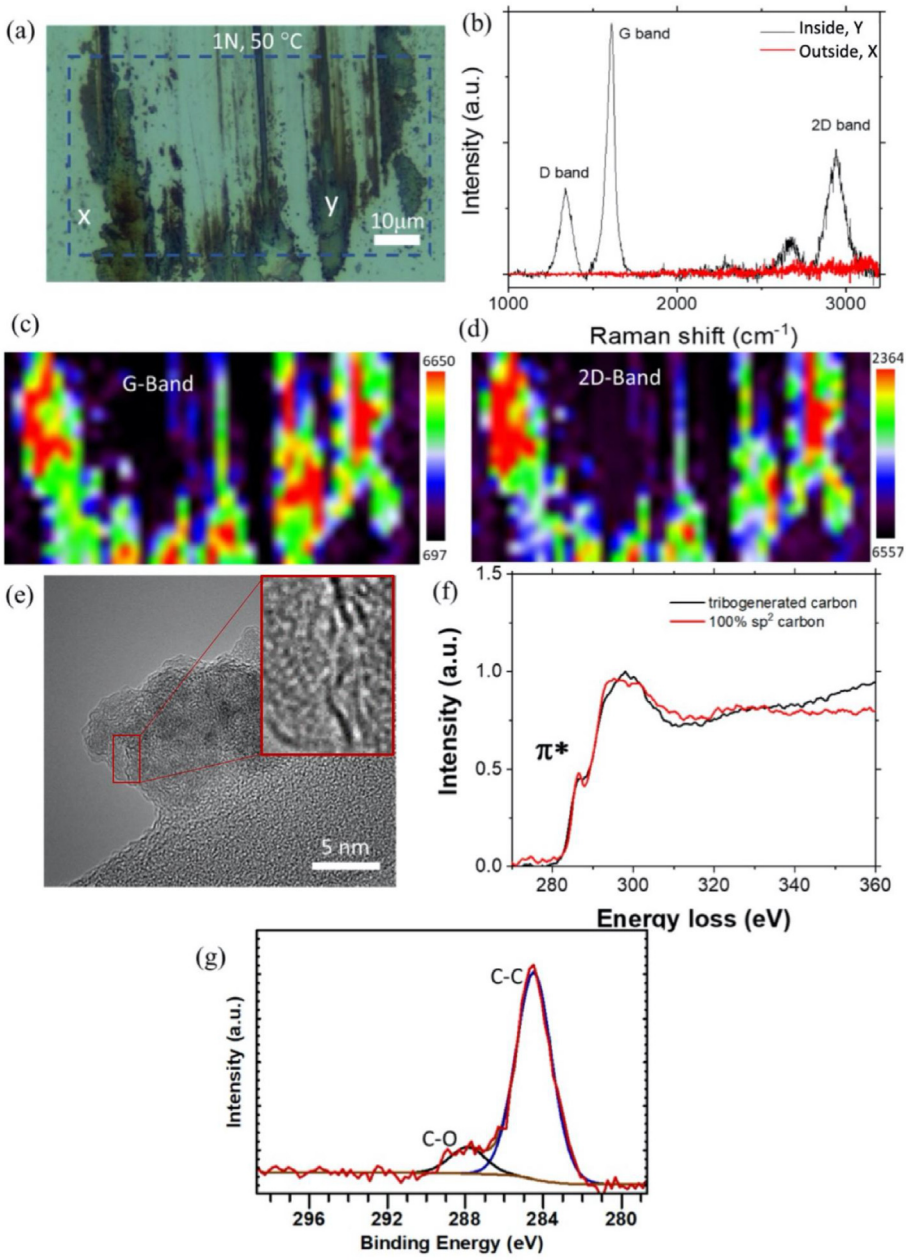

Fig. 5. (a) Optical micrographs of the wear track tested at 1 N, 50 °C. A designated area with the blue dashed line was used to perform Raman 2D mapping. (b) Single Raman spectra outside and inside the wear track, marked by "x" and "y" on (a). (c) Raman 2D mapping of G-band (at ~1560 cm^{-1} and (d) 2D-band (at ~2700 cm^{-1}) (e) TEM and (f) EELS analysis of the wear debris collected from the tribofilm (g) XPS analysis of the wear track.

growth species (for the carbon-based film growth $V_m = 5.29\ cm^3/mol$). The attempt frequency υ was selected $10^{13}\ s^{-1}$ [36]. Fitting the experimental data with the Arrhenius model provides the values of the fitting parameters ΔU_{act}, and ΔV_{act} as 0.96 eV, and 0.307 Å^3, respectively. These activation energy and activation volume values are of a similar range as the ones reported in prior studies focusing on mechanochemically induced tribofilm formation from organic species such as methyl thiolate, n-decane, or allyl alcohol vapor [37–39]. It should be noted that the recent numerical models suggested that the driving force for the reaction is the involved shear stress, though it is challenging to separate the effects of normal and shear stresses [40]. Considering this assumption, the activation volume would increase to ~2–3 Å^3 which is in agreement with the volume of the ethanol molecules and its covalent bond fragments potentially involved in the reaction.

EDS mapping of the wear tracks formed on the Pt-Au surface during sliding (Fig. 4) reveals the carbon-based nature of the formed tribo-film. The results suggest that the formation of these tribo-active-films highly depends on the applied load and temperature. The ratio of wt% of C relative to wt% of Pt is used to evaluate the progression in the carbon formation as a function of the testing parameters. Direct comparison between 25 °C and 50 °C at 0.25 N and 1 N load, indicates that at 0.25 N at 25 °C the C/Pt ratio is 0.07, with no clear carbon contrast inside the wear track, while at 1 N at 50 °C this ratio increases to 0.16, with clear carbon presence inside the wear track.

FIB cross-sectional image of the produced tribo-active film (Fig. 4e), shown by the red line in Fig. 4d, shows the adhesion of Pt-Au to the Cu substrate. Also, the thickness of the Pt-Au remains uniform and shows no evidence of severe plastic deformation or debris formation. Meanwhile, the cross-sectional images performed on the wear track formed during sliding at 1 N at 50 °C indicate the formation of non-uniform carbon film with a thickness of 100–200 nm, in agreement with the stylus profilometry measurements (Fig. 3h) and previous studies [28].

Further analysis of the Pt-Au wear tracks with Raman spectroscopy has been performed to unravel the nature of carbon in the wear track (Fig. 5a–d). Analysis of the tribo-film shows clear G-band (at ~1560 cm^{-1}) and 2D-band (at ~2700 cm^{-1}) Raman peaks, indicating the formation of graphitic carbon [41]. 2D maps of these peaks indicate uniformity of the graphitic carbon inside the wear tracks. These results suggest that high contact pressure and elevated temperature at the sliding interface during tribotests in ethanol activate the tribocatalytically-induced transformation of carbon from the hydrocarbon source to graphitic carbon. The structure of the resulting carbon films is an important aspect to highlight. In our earlier studies, we observed the formation of DLC-like film tribocatalytically-induced from low-viscosity hydrocarbons by the presence of copper in the coating [24]. Therefore, Pt here plays the important role of the catalyst by not only inducing dehydrogenation but also reorganizing the released carbon atoms. As more sliding cycles pass, larger amounts of graphitic carbon are generated. The dynamic movement of the counter-part during the reciprocating sliding sweeps the graphitic film towards the edges of the wear track which leads to the observed nonuniformity of the carbon in the wear track.

HRTEM analysis of the wear debris collected from the wear track further reveals the nature of the carbon film (Fig. 5e). The generated tribofilm has an amorphous carbon structure with regions of layered films. Electron energy loss spectroscopy (EELS) analysis shows the presence of π* peak (pre-peak) before the major carbon peak (s peak) which is further indicative of the high amount of sp^2 carbon. The sp^2 ratio for the debris has been calculated by comparing the areas of the π* peak and total peak for the collected

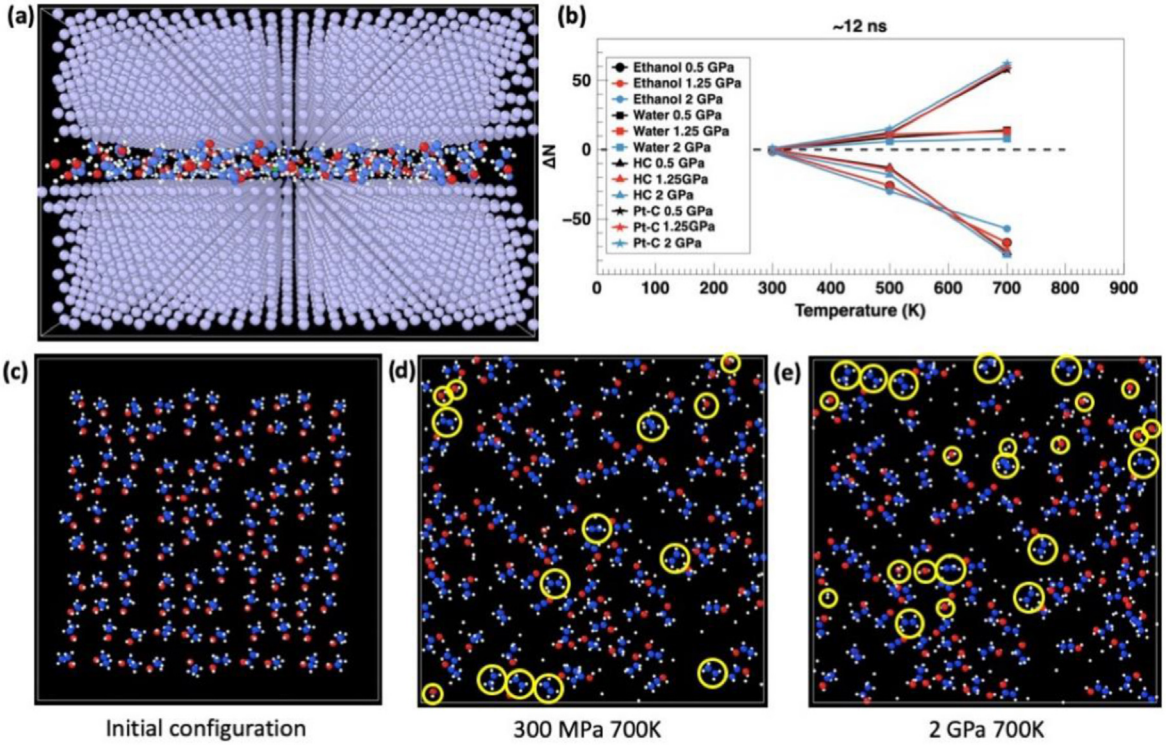

Fig. 6. MD simulation results. (a) Snapshot of the overall system. (b) Change in the number of bonds, ΔN, as a function of temperature and pressure after 12ns of simulation time. (c)–(e) top-down snapshots of the simulations (Pt removed) in the initial configuration (c) and after ~12 ns of shear at contact pressures of 700 K at 300 MPa (d) and 2 GPa (e). Molecular fragments in (d) and (e) are circled in yellow.

tribofilm to the reference spectra collected for a completely sp^2-bonded carbon, graphite:

$$R = \left(\frac{I_\pi}{I_t}\right) \div \left(\frac{I_\pi(g)}{I_t(g)}\right)$$

with I_π and $I_\pi(g)$ being the intensity of the π^* peak and I_t and $I_t(g)$ being the intensity of the $\pi^*$and s peaks integrated over a range of 50 eV for the analyzed sample and sp^2 reference, respectively [42]. The resulting amount of the sp^2 carbon for the tribofilm is approximately 86±3%.

XPS characterization of the wear track further confirms the dominancy of the C–C nature of the bonds in the formed carbon tribofilm, corresponding to the graphitic carbon. The presence of a small C–O peak can be associated with the partial oxidation of the graphitic flakes at the defects and edges upon exposure to the ethanol environment or ambient conditions post-experiment.

To probe the mechanisms involved in the formation of the graphitic carbon at the sliding interfaces we performed molecular dynamics (MD) simulations (Fig. 6). Ethanol molecules were compressed between two slabs of platinum (Fig. 6a) and sheared at 1 m/s for ~12 ns at temperatures of 300–700 K and normal loads of 0.5–2 GPa while tracking the change in the number of bonds, ΔN, during the simulation (Fig. 6b). The temperature values were selected based on previous studies [17,43,44] suggesting that under high contact pressure and shear, local asperity temperatures during sliding can be as high as 1773 K. Four different types of molecular fragments were counted; ethanol, water, H–C bonds, and Pt–C bonds. The results show that the ethanol molecules are dissociated during sliding, and form smaller molecular fragments, with an increase in the number of Pt–C bonds. Sutter et al. [45] previously demonstrated graphene growth from Pt–C upon cooling. As in the tribological tests, the sliding interfaces are dynamic, they experience not only local heating but also cooling enabling the transformation of Pt-C into graphene. At the same time, the H–C bonds of ethanol molecules are dissociated with increasing temperature and pressure, releasing hydrogen atoms and freeing carbons. Interestingly, the dissociation process results only in relatively small amounts of water. These results indicate that changing the temperature from 300 K to 700 K has a much stronger effect than increasing the contact pressure 4 times, from 0.5 GPa to 2 GPa (Fig. 6c–e). Such conclusion is in line with the experimental observations demonstrating high sensitivity of the tribofilm formation to the temperature increase.

5. Conclusion

Hard and wear-resistant Pt-Au films were deposited on Cu substrates. NanoSEM, AFM, and top-view TEM show a columnar structure through the thickness of the film with ~30 nm average grain size. Au-EDS map of the top-view TEM analysis illustrates the segregation of gold along the grain boundaries that provides improved mechanical properties.

Tribological testing of the Pt-Au film and AISI 440C HT steel in an ethanol environment shows three orders of magnitude difference in the wear rate of the materials. Detailed tribological experiments with 0.25–1 N applied load and at 25 °C and 50 °C indicate tribofilm formation in the wear track. Results indicate that load and temperature affect the tribo-film formations. The observed tribofilm growth rate is fitted to an Arrhenius equation, indicating an increase in the film formation with applied load and higher temperature.

EDS analysis indicates the formation of a carbon-based tribofilm with a tendency to accumulate at the ends of the wear track. FIB-SEM cross-section analysis confirms a film of 100–200 nm thickness without any signs of severe plastic deformation in the contact. 2D-Raman spectroscopy reveals that tribo-generated film is mostly graphitic carbon with strong G-band and 2D-band peaks. HRTEM characterization reveals the amorphous structure of the tribo-generated carbon in the wear track. TEM-EELS and XPS analyses provide more evidence that tribo-active carbon film has sp^2 bonding. MD simulations further support these findings and indicate a strong effect of temperature on the dissociation of ethanol molecules, necessary for the formation of the graphitic tribofilms.

Credit statement

Asghar Shirani: Investigation, Data Curation, Writing. **Yuzhe Li:** Investigation, Data Curation. **Jesse Smith:** Data Curation. **John F. Curry**: Resources, Writing. **Ping Lu:** Data Curation. **Mark Wilson:** Data Curation. **Michael Chandross**: Investigation, Writing. **Nicolas Argibay:** Resources. **Diana Berman:** Supervision, Investigation, Conceptualization, Writing.

Declaration of competing interest

The authors declare that they have no known competing financial interests or personal relationships that could have appeared to influence the work reported in this paper.

Data availability

Data will be made available on request.

Acknowledgments

The authors acknowledge the support of this work by the National Science Foundation (NSF) (Award No. 2018132). This work was funded by the LDRD program at Sandia National Laboratories, a multi-mission laboratory managed and operated by National Technology and Engineering Solutions of Sandia, LLC, a wholly-owned subsidiary of Honeywell International, Inc., for the U.S. Department of Energy's National Nuclear Security Administration under Contract No. DE- NA0003525. Any subjective views or opinions that might be expressed in the paper do not necessarily represent the views of the U.S. Department of Energy or the United States Government.

References

[1] R. Kurz, K. Brun, Degradation in gas turbine systems, J. Eng. Gas Turbines Power 123 (2000) 70–77.
[2] A. Greco, S. Sheng, J. Keller, A. Erdemir, Material wear and fatigue in wind turbine systems, Wear 302 (2013) 1583–1591.
[3] E.R. Booser, Tribology Data Handbook: an Excellent Friction, Lubrication, and Wear Resource, CRC Press, 1997.
[4] S.-T. Buljan, S.F. Wayne, Wear and design of ceramic cutting tool materials, Wear 133 (1989) 309–321.
[5] E.J. Breton, J.M. Handzel, O.K. Tennant, Process for Making Wear-Resistant Coatings, Google Patents, 2003.
[6] S.J. Mroczkowski, Multi-layer Wear Resistant Coatings, Google Patents, 1990.
[7] M. Marian, D. Berman, A. Rota, R.L. Jackson, A. Rosenkranz, Layered 2D nanomaterials to tailor friction and wear in machine elements—a review, Adv. Mater. Interfac. 9 (2022), 2101622.
[8] D. Berman, A. Erdemir, A.V. Sumant, Graphene as a protective coating and superior lubricant for electrical contacts, Appl. Phys. Lett. 105 (2014), 231907.
[9] D. Berman, S.A. Deshmukh, S.K.R.S. Sankaranarayanan, A. Erdemir, A.V. Sumant, Extraordinary macroscale wear resistance of one atom thick graphene layer, Adv. Funct. Mater. 24 (2014) 6640–6646.
[10] D. Berman, A. Erdemir, A.V. Sumant, Reduced wear and friction enabled by graphene layers on sliding steel surfaces in dry nitrogen, Carbon 59 (2013) 167–175.
[11] D. Berman, A. Erdemir, A.V. Sumant, Few layer graphene to reduce wear and friction on sliding steel surfaces, Carbon 54 (2013) 454–459.
[12] C. Soldano, A. Mahmood, E. Dujardin, Production, properties and potential of graphene, Carbon 48 (2010) 2127–2150.

[13] D. Prasai, J.C. Tuberquia, R.R. Harl, G.K. Jennings, K.I. Bolotin, Graphene: corrosion-inhibiting coating, ACS Nano 6 (2012) 1102–1108.
[14] C. Lee, X. Wei, J.W. Kysar, J. Hone, Measurement of the elastic properties and intrinsic strength of monolayer graphene, Science 321 (2008) 385–388.
[15] G.-H. Lee, R.C. Cooper, S.J. An, S. Lee, A. van der Zande, N. Petrone, A.G. Hammerberg, C. Lee, B. Crawford, W. Oliver, J.W. Kysar, J. Hone, High-strength chemical-vapor–deposited graphene and grain boundaries, Science 340 (2013) 1073–1076.
[16] A. Ayyagari, K.I. Alam, D. Berman, A. Erdemir, Progress in superlubricity across different media and material systems-A review, Front. Mech. Eng. 67 (2022).
[17] M.F. Ashby, J. Abulawi, H.S. Kong, Temperature maps for frictional heating in dry sliding, Tribol. Trans. 34 (1991) 577–587.
[18] T.D.B. Jacobs, R.W. Carpick, Nanoscale wear as a stress-assisted chemical reaction, Nat. Nanotechnol. 8 (2013) 108–112.
[19] Y. Junbin, D. Junxiu, Tribocatalysis reaction during antiwear synergism between borates and Sn(IV) compounds in boundary lubrication, Tribol. Int. 29 (1996) 429–432.
[20] T. Onodera, K. Kawasaki, T. Nakakawaji, Y. Higuchi, N. Ozawa, K. Kurihara, M. Kubo, Tribocatalytic reaction of polytetrafluoroethylene sliding on an Aluminum surface, J. Phys. Chem. C 119 (2015) 15954–15962.
[21] Q. Chen, D. Li, A computational study of frictional heating and energy conversion during sliding processes, Wear 259 (2005) 1382–1391.
[22] C. Kajdas, K. Hiratsuka, Tribochemistry, tribocatalysis, and the negative-ion-radical action mechanism, Proc. IME J. J. Eng. Tribol. 223 (2009) 827–848.
[23] P. Ren, K. Zhang, X. He, S. Du, X. Yang, T. An, M. Wen, W. Zheng, Toughness enhancement and tribochemistry of the Nb-Ag-N films actuated by solute Ag, Acta Mater. 137 (2017) 1–11.
[24] A. Shirani, Y. Li, O.L. Eryilmaz, D. Berman, Tribocatalytically-activated formation of protective friction and wear reducing carbon coatings from alkane environment, Sci. Rep. 11 (2021), 20643.
[25] K. Gao, B. Wang, A. Shirani, Q. Chang, D. Berman, Macroscale superlubricity accomplished by Sb2O3-MSH/C under high temperature, Front. Chem. 9 (2021) 226.
[26] D. Berman, A. Erdemir, Achieving ultralow friction and wear by tribocatalysis: enabled by in-operando formation of nanocarbon films, ACS Nano 15 (2021) 18865–18879.
[27] Y. Liao, R. Pourzal, M.A. Wimmer, J.J. Jacobs, A. Fischer, L.D. Marks, Graphitic tribological layers in metal-on-metal hip replacements, Science 334 (2011) 1687–1690.
[28] N. Argibay, T.F. Babuska, J.F. Curry, M.T. Dugger, P. Lu, D.P. Adams, B.L. Nation, B.L. Doyle, M. Pham, A. Pimentel, C. Mowry, A.R. Hinkle, M. Chandross, In-situ tribochemical formation of self-lubricating diamond-like carbon films, Carbon 138 (2018) 61–68.
[29] A. Erdemir, G. Ramirez, O.L. Eryilmaz, B. Narayanan, Y. Liao, K. Ganesh, S.K.R.S. Sankaranarayanan, Carbon-based tribofilms from lubricating oils, Nature 536 (2016) 67–71.
[30] D. Berman, K.C. Mutyala, S. Srinivasan, S.K.R.S. Sankaranarayanan, A. Erdemir, E.V. Shevchenko, A.V. Sumant, Iron-nanoparticle driven tribochemistry leading to superlubric sliding interfaces, Adv. Mater. Interfac. 6 (2019), 1901416.
[31] J.F. Curry, T.F. Babuska, T.A. Furnish, P. Lu, D.P. Adams, A.B. Kustas, B.L. Nation, M.T. Dugger, M. Chandross, B.G. Clark, Achieving ultralow wear with stable nanocrystalline metals, Adv. Mater. 30 (2018), 1802026.
[32] A.P. Thompson, H.M. Aktulga, R. Berger, D.S. Bolintineanu, W.M. Brown, P.S. Crozier, P.J. in 't Veld, A. Kohlmeyer, S.G. Moore, T.D. Nguyen, R. Shan, M.J. Stevens, J. Tranchida, C. Trott, S.J. Plimpton, LAMMPS - a flexible simulation tool for particle-based materials modeling at the atomic, meso, and continuum scales, Comput. Phys. Commun. 271 (2022), 108171.
[33] Y.K. Shin, L. Gai, S. Raman, A.C.T. van Duin, Development of a ReaxFF reactive force field for the Pt–Ni alloy catalyst, J. Phys. Chem. A 120 (2016) 8044–8055.
[34] F. Abdeljawad, P. Lu, N. Argibay, B.G. Clark, B.L. Boyce, S.M. Foiles, Grain boundary segregation in immiscible nanocrystalline alloys, Acta Mater. 126 (2017) 528–539.
[35] H. Fujita, H. Spikes, The formation of zinc dithiophosphate antiwear films, Proc. IME J. J. Eng. Tribol. 218 (2004) 265–278.
[36] N.N. Gosvami, J.A. Bares, F. Mangolini, A.R. Konicek, D.G. Yablon, R.W. Carpick, Mechanisms of antiwear tribofilm growth revealed in situ by single-asperity sliding contacts, Science 348 (2015) 102–106.
[37] H.L. Adams, M.T. Garvey, U.S. Ramasamy, Z. Ye, A. Martini, W.T. Tysoe, Shear-induced mechanochemistry: pushing molecules around, J. Phys. Chem. C 119 (2015) 7115–7123.
[38] J. Yeon, X. He, A. Martini, S.H. Kim, Mechanochemistry at solid surfaces: polymerization of adsorbed molecules by mechanical shear at tribological interfaces, ACS Appl. Mater. Interfaces 9 (2017) 3142–3148.
[39] X. He, S.H. Kim, Mechanochemistry of physisorbed molecules at tribological interfaces: molecular structure dependence of tribochemical polymerization, Langmuir 33 (2017) 2717–2724.
[40] H. Spikes, Stress-augmented thermal activation: tribology feels the force, Friction 6 (2018) 1–31.
[41] A.C. Ferrari, Raman spectroscopy of graphene and graphite: disorder, electron–phonon coupling, doping and nonadiabatic effects, Solid State Commun. 143 (2007) 47–57.
[42] L. Wan, R. Egerton, Preparation and characterization of carbon nitride thin films, Thin Solid Films 279 (1996) 34–42.
[43] B. Bhushan, Modern Tribology Handbook, Two Volume Set, CRC Press, 2000.
[44] W. Qin, X. Jin, A. Kirk, P.H. Shipway, W. Sun, Effects of surface roughness on local friction and temperature distributions in a steel-on-steel fretting contact, Tribol. Int. 120 (2018) 350–357.
[45] P. Sutter, J.T. Sadowski, E. Sutter, Graphene on Pt (111): growth and substrate interaction, Phys. Rev. B 80 (2009), 245411.